Developmental Cell
Article

CHD5 Is Required for Neurogenesis and Has a Dual Role in Facilitating Gene Expression and Polycomb Gene Repression

Chris M. Egan,[1,9] Ulrika Nyman,[7,9] Julie Skotte,[3] Gundula Streubel,[1] Siobhán Turner,[1] David J. O'Connell,[6] Vilma Raklli,[7] Michael J. Dolan,[1] Naomi Chadderton,[1] Klaus Hansen,[3] Gwyneth Jane Farrar,[1] Kristian Helin,[3,4,5] Johan Holmberg,[7,8,10,*] and Adrian P. Bracken[1,2,10,*]

[1]The Smurfit Institute of Genetics, Trinity College Dublin, Dublin 2, Ireland
[2]The Adelaide and Meath Hospital, Incorporating the National Children's Hospital, Dublin 16, Ireland
[3]Biotech Research and Innovation Centre (BRIC)
[4]Centre for Epigenetics
[5]The Danish Stem Cell Center (DanStem)
University of Copenhagen, 2200 Copenhagen, Denmark
[6]The Conway Institute, University College Dublin, Dublin 4, Ireland
[7]Ludwig Institute for Cancer Research
[8]Department of Cell and Molecular Biology
Karolinska Institutet, Stockholm S-171 77, Sweden
[9]These authors contributed equally to this work
[10]These authors contributed equally to this work
*Correspondence: johan.holmberg@licr.ki.se (J.H.), adrian.bracken@tcd.ie (A.P.B.)
http://dx.doi.org/10.1016/j.devcel.2013.07.008

SUMMARY

The chromatin remodeler CHD5 is expressed in neural tissue and is frequently deleted in aggressive neuroblastoma. Very little is known about the function of CHD5 in the nervous system or its mechanism of action. Here we report that depletion of *Chd5* in the developing neocortex blocks neuronal differentiation and leads to an accumulation of undifferentiated progenitors. CHD5 binds a large cohort of genes and is required for facilitating the activation of neuronal genes. It also binds a cohort of Polycomb targets and is required for the maintenance of H3K27me3 on these genes. Interestingly, the chromodomains of CHD5 directly bind H3K27me3 and are required for neuronal differentiation. In the absence of CHD5, a subgroup of Polycomb-repressed genes becomes aberrantly expressed. These findings provide insights into the regulatory role of CHD5 during neurogenesis and suggest how inactivation of this candidate tumor suppressor might contribute to neuroblastoma.

INTRODUCTION

The process of neurogenesis is characterized by a gradual loss of progenitor properties and the acquisition of specific neuronal traits (Molyneaux et al., 2007). This is accompanied by a progressive restriction on possible alternative cellular fates. The instructive and inductive roles played by DNA-binding transcription factors in the acquisition of differentiated neuronal properties are well characterized (Bertrand et al., 2002; Molyneaux et al., 2007). However, less is known about how gene programs of alternative lineages are silenced. Furthermore, the precise roles of chromatin regulators during neuronal lineage specification remain largely unexplored.

Chromatin regulators are generally considered to act as facilitators of lineage specification, rather than actually directing the process (Holmberg and Perlmann, 2012). Several different classes of chromatin regulators, such as those involved in "writing" and "reading" histone posttranslational modifications, have been shown to be centrally involved in gene expression control during lineage specification (Kouzarides, 2007; Schübeler, 2009). For example, the Polycomb and Trithorax group proteins are very well characterized regulators of cell-fate decisions that act antagonistically during development (Bracken and Helin, 2009; Pietersen and van Lohuizen, 2008). EZH2, a component of Polycomb Repressive Complex 2 (PRC2), is a "writer" protein that, together with SUZ12 and EED, mediates trimethylation of histone H3 at lysine 27 (H3K27me3), a mark associated with gene repression (Margueron and Reinberg, 2011). In contrast, several writers within the Trithorax family mediate the deposition of H3K4me3, a mark generally associated with gene activation (Schuettengruber et al., 2011). Chromatin "reader" proteins regulate gene expression by binding to, or reading, posttranslationally modified histone proteins (Taverna et al., 2007). Their interactions with histone N-terminal tails are mediated by conserved structural domains such as chromodomains, plant homeodomains (PHDs), and Tudor domains (Yap and Zhou, 2010).

The CHD1–9 family of reader proteins is defined by the presence of two N-terminal chromodomains and a helicase-like ATPase motif associated with nucleosome remodeling (Clapier and Cairns, 2009). Several members of this family have been suggested to play key roles during development (Ho and Crabtree, 2010). For example, CHD1 has a crucial role in regulating embryonic stem cell (ESC) pluripotency by maintaining the "open chromatin state" that is characteristic of pluripotent cells (Gaspar-Maia et al., 2009). This function of CHD1 is partly

associated with the ability of its tandem chromodomains to bind to H3K4me3 (Flanagan et al., 2005; Simic et al., 2003). Similarly, CHD7 binds H3K4me1 via its chromodomains and has been reported to be required for controlling the active state of distal enhancer elements within the neural crest lineage (Bajpai et al., 2010; Schnetz et al., 2009).

CHD reader proteins in the CHD3–5 subgroup are uniquely defined by their double PHD domains, in addition to their double chromodomains (see Figure 4A). Although the PHD domains of CHD4 and CHD5 have been shown to bind unmodified H3K4, very little is known about the histone-binding specificity of the double chromodomains of these proteins (Musselman et al., 2009; Paul et al., 2013). Both CHD3 and CHD4 are members of the multiprotein nucleosome remodeling and deacetylase (NuRD) complex, which was originally identified as a transcriptional repressor (McDonel et al., 2009). Interestingly, the histone deacetylation activity of CHD4 NuRD-containing complexes was recently shown to facilitate the recruitment of PRC2 components and subsequent deposition of H3K27me3 at target genes (Reynolds et al., 2012). Consistent with this, dMI-2, the closest CHD3–5 protein homolog in *Drosophila*, synergizes with Polycomb group proteins to maintain the repressed state of certain homeotic genes during larval development (Kehle et al., 1998). However, other studies suggest that the CHD3–4 proteins may also modulate transcription at active genes (Reynolds et al., 2013). For example, the dMI-2 protein colocalizes with RNA Polymerase II on sites of actively transcribed genes in *Drosophila* (Murawska et al., 2008), and chromatin immunoprecipitation sequencing (ChIP-seq) analysis of CHD4 indicates that it binds to the gene loci of a large number of active genes in mouse ESCs and lymphocytic progenitor cells (Hu and Wade, 2012).

The *CHD5* gene resides within a chromosomal region spanning 23 genes at 1p36, which commonly exhibits loss of heterozygosity in high-risk neuroblastoma (Brodeur, 2003; Okawa et al., 2008). In fact, *CHD5* has been proposed to be the key tumor-suppressor gene within this locus (Bagchi et al., 2007). Neuroblastomas are thought to originate from neural-crest-derived precursor cells of the sympathetic neuronal lineage (Brodeur, 2003). CHD5 is expressed in normal neuronal tissues and in low-risk neuroblastomas, but its expression levels are significantly reduced in tumors from high-risk neuroblastoma patients (Fujita et al., 2008; Garcia et al., 2010). Notably, ectopic expression of CHD5 abrogates the growth of neuroblastoma cell lines both in vitro and in xenografts (Fujita et al., 2008). However, very little is known about the role of CHD5 during neuronal differentiation, and in particular, how its loss might contribute to the development of neuroblastoma. In this study, we show that CHD5 is required for terminal neuronal differentiation and has a dual role in facilitating both the activation of neuronal genes and the repression of a cohort of Polycomb target genes.

RESULTS

Expression of Chd5 Is Activated in Late-Stage Progenitors and Is Maintained in Terminally Differentiated Neurons

Previously, CHD5 was shown to be predominantly expressed in the adult CNS (Garcia et al., 2010; Potts et al., 2011). To further evaluate its pattern of expression, we performed quantitative RT-PCR (qRT-PCR) and western blot analysis in multiple mouse tissue types, and found it to be expressed in the brain and, albeit to a lesser degree, in the retina and adrenal gland (Figures 1A and 1B). To acquire a detailed view of the spatial distribution and cell-type specificity of *Chd5* expression, we developed CHD5-specific antibodies for immunofluorescent staining (Figures S1A–S1C available online) and observed abundant nuclear CHD5 staining in NEUN$^+$ neurons of the neocortex (Figure 1C), but not in surrounding astrocytes or oligodendrocytes (Figures 1D and 1E). A neuron-specific staining pattern was also observed in both the retina (Figure S1D) and adrenal gland, where CHD5 immunoreactivity is restricted to TUJ1$^+$ neuroendocrine cells (Figure 1F; Figure S1E). The pattern of *Chd5* expression suggests that CHD5 is a neuron-specific chromatin remodeler with roles in both the CNS and peripheral tissues of neural origin.

In order to explore the temporal onset of CHD5 expression during adult neurogenesis, we performed immunofluorescent staining in the adult mouse hippocampus, where we observed an extensive overlap of CHD5 with NEUN (Figure 1G). A minor population of CHD5-positive cells lacking NEUN staining was also detected (Figure 1G, inset). The position in the neurogenic subgranular zone (SGZ) suggested that these cells were neuronal progenitors. To determine the identity of these cells, we performed staining with antibodies specific for different progenitor states (Figures 1H–1K). We observed no overlap between CHD5 and the early SGZ type 1 stem cell marker, GFAP (Figure 1H). However, a significant number of CHD5 expressing cells also expressed high levels of DCX (Figure 1I), a marker for the type 2b and type 3 intermediate- to late-stage progenitors (Breunig et al., 2007). Because DCX expression persists in postmitotic immature granule cells (GCs), we also stained for the mitotic marker phospho-histone 3 (pH3). The colocalization of pH3 and DCX in a subpopulation of the CHD5-positive cells suggests a late-stage progenitor identity for this cell population (Figure S1F). Supporting this, we detected a subpopulation of CHD5-expressing cells, which also expressed the neural progenitor marker SOX3 (Figure 1J). Triple staining of bromodeoxyuridine (BrdU) pulse chase experiments confirmed that a cohort of the CHD5$^+$/SOX3$^+$ cell population had incorporated BrdU 24 hr after injection (Figure 1K), suggesting that this cell population had exited the cell cycle in the previous 24 hr. The lack of BrdU staining in animals sacrificed 2 hr after BrdU injection (data not shown) implies that CHD5 is not expressed in rapidly proliferating progenitors. Taken together, these data suggest that CHD5 is upregulated during terminal differentiation of late-stage neuronal progenitors.

Chd5 Is Required for Terminal Differentiation of Embryonic Cortical Neurons

We next wished to investigate the role of CHD5 during embryonic neurogenesis. The vast majority of murine cortical neurons are generated between embryonic day 10 (E10) and E18 (Molyneaux et al., 2007). Consistent with our observations in the adult CNS, we found CHD5 to be expressed throughout cortical and spinal cord development as cells downregulated progenitor properties, exited the cell cycle, and acquired a terminally differentiated neuronal identity (Figure 1L; Figures S2A–S2D).

To analyze the consequences of *Chd5* knockdown in the developing neocortex, we designed two GFP-expressing small

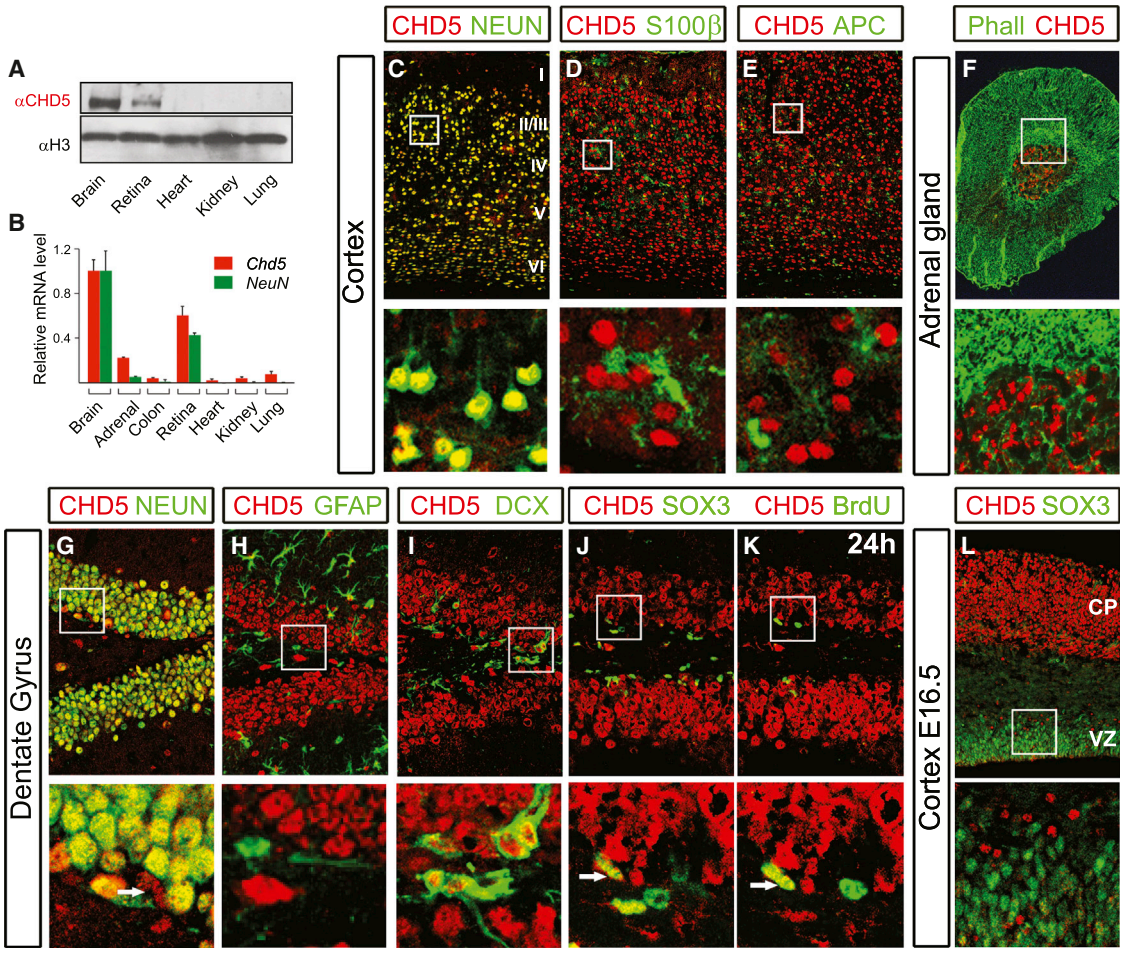

Figure 1. CHD5 Is a Pan-Neuronal Marker that Is Upregulated during Late-Stage Neurogenesis

(A) Western blot of CHD5 and histone H3 in tissues derived from P10 mice pups.

(B) qRT-PCR of *Chd5* and NeuN (*Fox-3*) mRNA levels in tissues from P10 mice pups. Error bars indicate the SD of triplicate qPCR data.

(C–E) Staining in the adult mouse cortex of CHD5 (red) and the neuronal marker NEUN (green in C), the astrocytic marker S100B (green in D), and the oligodendrocytic marker APC (green in E).

(F) CHD5 protein (red) specifically localizes to the neuroendocrine portion of the adrenal gland. Phalloidin (green) staining is used to discriminate between the adrenal medulla and the actin-rich adrenal cortex.

(G) The majority of CHD5$^+$ cells (red) in the DG of the hippocampus are differentiated NeuN$^+$ (green) neurons. The inset shows that a small subpopulation of Chd5$^+$ cells is NEUN$^-$ (arrow in inset).

(H) GFAP$^+$ (green) astrocytes or stem cells in the DG are CHD5$^-$ (red).

(I) A subpopulation of DCX$^+$ (green) progenitor cells are also CHD5$^+$ (red).

(J) Several SOX3$^+$ (green) neural stem/progenitor cells are also CHD5$^+$ (red).

(K) A subpopulation of the SOX3$^+$/CHD5$^+$ cells in (J) have incorporated BrdU (green) after a 24 hr pulse chase experiment (arrows in insets J and K).

(L) Prominent CHD5 (red) expression is evident in the CP of E16.5 mouse neocortex, but not in the majority of SOX3$^+$ (green) stem cells of the VZ.

CP, cortical plate; DG, dentate gyrus; VZ, ventricular zone. See also Figure S1.

hairpin RNA (shRNA) vectors (*shChd5.1* and *shChd5.2*) directed against *Chd5*. We electroporated them or a *shCtrl-Gfp* control vector in utero into the developing E14.5 cortex and subsequently analyzed the embryos at E18.5 (Figure 2; Figures S2E and S2F). In the embryos electroporated with *shCtrl-Gfp*, GFP-positive cells were distributed along the growing cortex from the ventricular zone (VZ) all the way out to the pial surface, and the majority expressed CHD5 (Figure 2A). In contrast, in *shChd5.1-Gfp* or *shChd5.2-Gfp* electroporated cortices, a near complete lack of overlap between GFP and CHD5 was evident, indicating efficient knockdown of CHD5 (Figures 2B and 2C; data not shown). The knockdown of CHD5 was accompanied by a severe failure of cells to exit the germinal VZ, SVZ, and intermediate zone (Figures 2B). In the *shCtrl-Gfp* embryos, the overlap with SOX3 was minimal, whereas among the *shChd5-Gfp* electroporated cells, almost 30% were SOX3$^+$ (Figures 2D–2F). In addition, there was a slight but significant increase in the number of cells expressing the cell-cycle marker KI67 in the *shChd5.1-Gfp* electroporated cells (Figures 2G–2I). The deeper cortical layers V–VI are generated earlier than the electroporated cells. Accordingly, a cohort of *shCtrl-Gfp*-expressing cells migrated through these deep layers without expressing the

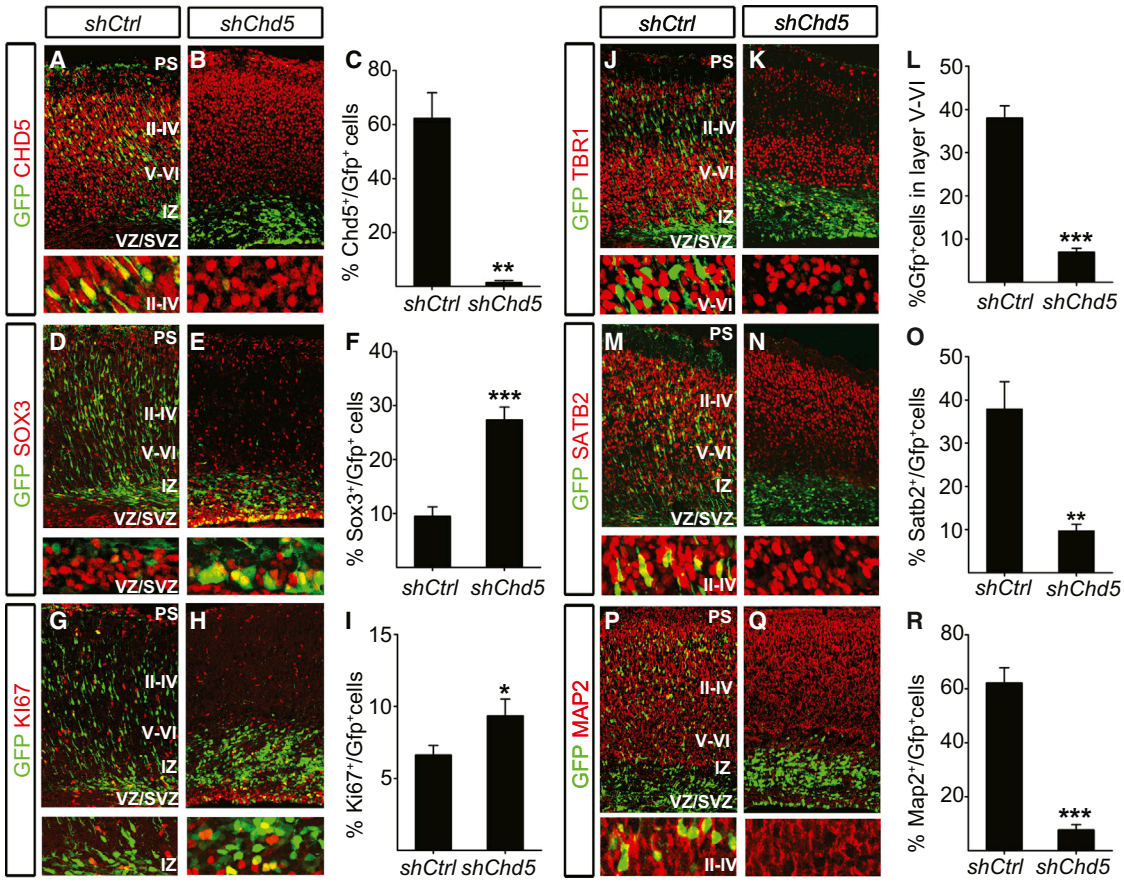

Figure 2. CHD5 Is Required for Neuronal Differentiation of Embryonic Cortical Neurons

(A) In utero electroporated *shCtrl-Gfp* expressing cells (green) exit the VZ/SVZ, migrate out into the cortical layers, and upregulate CHD5 (red) expression.

(B) Cells electroporated with *shChd5-Gfp* (green) remain in the VZ/SVZ or IZ and do not upregulate CHD5.

(C) Quantification of *shCtrl-Gfp* and *shChd5-Gfp* electroporated cells in utero, displaying the percentage of GFP-positive cells that are also positive for CHD5.

(D and E) *ShCtrl-Gfp*-expressing cells downregulate the neural stem/progenitor cell marker SOX3 (red, E) as they exit the VZ/SVZ (D). A significant proportion of *shChd5-Gfp*-expressing cells (green) retain expression of SOX3 (red).

(F) Quantification of the percentage of $GFP^+/SOX3^+$ cells in *shCtrl* and *shChd5-Gfp* electroporated mice.

(G–I) An increased number of $KI67^+$ cells (red) in *shChd5-Gfp* expressing cells (H and I) in comparison to control electroporated cells (G and I).

(J and K) Cell migration through the $TBR1^+$ (red) deeper layers V–VI was unperturbed in the *shCtrl* electroporated embryos (J), but significantly reduced in *shChd5-Gfp* electroporated embryos (K).

(L) Quantification of the percentage of GFP^+ cells migrating through V–VI.

(M) The *shCtrl-Gfp* electroporated cells (green) reach layers II–IV and upregulate expression of the layer-specific neuronal marker SATB2 (red).

(N) The *shChd5-Gfp* electroporated cells (green) remain in the IZ/SVZ/VZ, not expressing SATB2 (red).

(O) Quantification of the percentage of GFP^+ cells that are $SATB2^+$.

(P) Robust expression of the pan-neuronal marker MAP2 (red) in the cells expressing *shCtrl-Gfp*.

(Q) Cells expressing *shChd5.2-Gfp* fail to upregulate MAP2 expression.

(R) Quantification of the percentage of GFP^+ cells that are $MAP2^+$.

IZ, intermediate zone; PS, pial surface; SVZ, subventricular zone; VZ, ventricular zone. Data are represented as mean ± SEM. *$p < 0.05$, **$p < 0.01$, ***$p < 0.001$, Student's t test, n = 4. See also Figure S2.

layer-specific marker TBR1 (Figure 2J). In contrast, the *shChd5.1-Gfp*-expressing cells showed significantly reduced migration through layers V–VI (Figures 2K and 2L).

A substantial number of the *shCtrl-Gfp*-expressing cells reached layers II–IV and expressed SATB2, a transcription factor that distinguishes these upper layers from the deeper layers (Figure 2M). However, virtually no cells expressing *shChd5.1-Gfp* reached layers II–IV, and consequently there was a significant reduction of $GFP^+/SATB2^+$ cells in layers II–IV (Figures 2N and 2O). We also stained with an antibody specific for the pan-neuronal protein MAP2 and observed an abundant colocalization of GFP and MAP2 in the control electroporated cortices (Figure 2P), whereas the *shChd5.1-Gfp* electroporated cortices displayed severely reduced numbers of GFP^+ cells that expressed MAP2 (Figures 2Q and 2R). This suggests that the defect is not the result of precocious generation of neurons within the germinal zone of the *shChd5.1-Gfp*-treated cortices or of defective radial migration. These undifferentiated cells also lacked detectable cleaved Caspase 3, suggesting that apoptotic pathways were not activated (data not shown). Taken

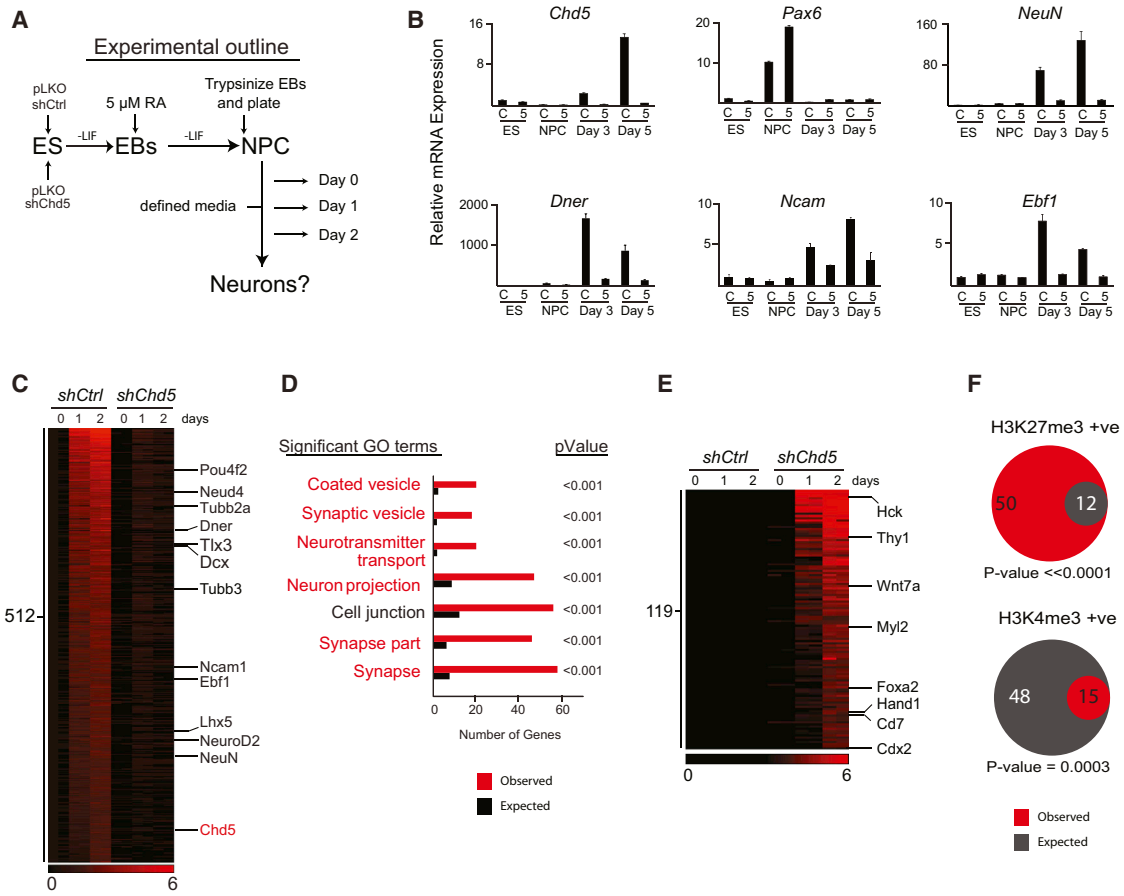

Figure 3. CHD5 Is Required during In Vitro Neurogenesis for Activation of the Neurogenic Gene Expression Program and the Maintained Repression of Polycomb Target Genes

(A) Flow diagram depicting the knockdown strategy for CHD5 in a model of in vitro derivation of CNS neurons from mouse E14 ESCs.

(B) qRT-PCR analysis of ESCs, NPCs (day 0), and cells during terminal differentiation (day 3 and day 5), infected with scrambled shRNA (C) or with a *Chd5* shRNA (5), showing the relative expression of *Chd5*, *Pax6* (a marker of neural progenitors), *Nanog* (a marker of ESCs), *NeuN* (a marker of neurons), *Dner*, *Ncam*, and *Ebf1*. Error bars indicate the SD of triplicate qPCR data.

(C) Tree-view representation of gene expression microarray data depicting the genes whose expression increases in *shCtrl*-infected cells, but not in *shChd5*-infected cells.

(D) GO analysis of the gene list from (C).

(E) Tree-view representation of gene expression microarray data depicting the genes whose expression increased in *shChd5*-infected cells, but not in *shCtrl*-infected cells.

(F) Venn diagram analysis representing a 4-fold enrichment of H3K27me3 promoter-positive genes in the cohort of genes upregulated in *Chd5*-depleted cells (E). The expected values were calculated based on a previously reported genome-wide data set (Mohn et al., 2008).

See also Figure S3.

together, these data demonstrate that CHD5 is required for terminal neuronal differentiation and that cells lacking appropriate CHD5 levels remain within the progenitor zone, retaining key progenitor properties.

Knockdown of Chd5 Results in Failure to Upregulate Neuronal Genes

To address the mechanisms by which CHD5 facilitates neuronal differentiation, we used an in vitro model of neurogenesis (Figure S3A; Bibel et al., 2007). *Chd5* messenger RNA (mRNA) expression increased during differentiation of mouse ESCs into neurons (Figures S3B and S3C), consistent with our in vivo observations. We next transduced ESCs with either *shCtrl* or one of two *Chd5* targeting vectors, *shChd5*, and induced cells to undergo neurogenesis (Figure 3A). The ESCs infected with *shChd5*, were capable of differentiating toward neural progenitor cells (NPCs), as indicated by the upregulation of *Pax6*. However, the reduced levels of *Chd5* led to a failure to further differentiate into neurons and this correlated with a failure to activate the expression of several canonical neuronal genes, including *Tubb3*, *NeuN* (*Fox-3*), and *Ncam* (Figure 3B). To understand the genome-wide consequences of *Chd5* knockdown during neuronal differentiation, we performed expression microarrays of *shCtrl*- and *shChd5*-infected cells (Figure 3C). This revealed that 512 genes were activated in control cells but not in the *Chd5*-depleted cells. A Gene Ontology (GO) analysis of these

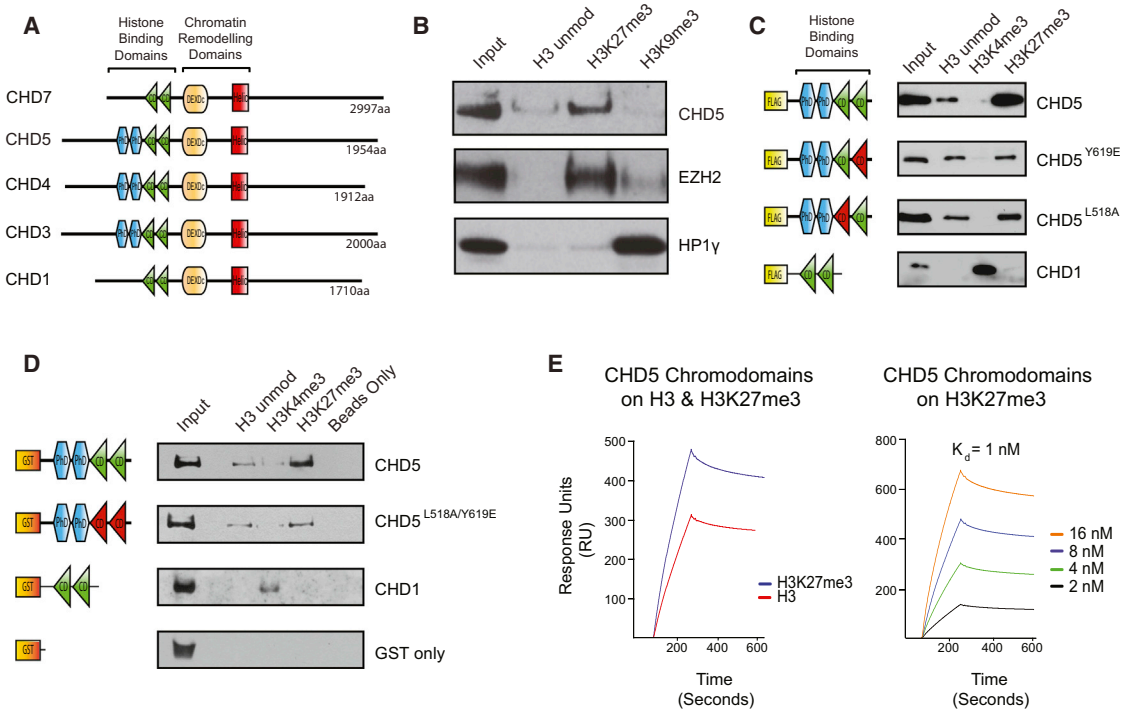

Figure 4. CHD5 Binds to the Polycomb-Mediated H3K27me3 Mark via Its Tandem Chromodomains

(A) Organization of the conserved domains within five distinct chromodomain helicase DNA-binding (CHD) proteins.

(B) Characterization of the association of the CHD5 protein with modified histone tails. Peptide pull-downs were performed on mouse brain nuclear lysates using biotin-tagged modified histone H3 peptides. Western blots were performed for CHD5, EZH2, and HP1γ as indicated.

(C) Peptide pull-downs of recombinant Flag-tagged wild-type and mutant histone-binding domain fragments of CHD5 and CHD1 expressed in HEK293 cells.

(D) Peptide pull-downs of recombinant GST-tagged wild-type and mutant histone-binding domain fragments of CHD5 and CHD1.

(E) Representative SPR sensorgrams for a GST-tagged peptide corresponding to the double-chromodomain portion of the CHD5 protein on both unmodified H3 peptides and H3K27me3-modified peptides. The affinity rate constants were determined from a concentration series of wild-type CHD5 fragment binding to H3K27me3.

See also Figure S4.

genes revealed a striking enrichment of factors involved in late-stage neuronal differentiation (Figure 3D). This included genes with roles in the regulation of synapse development, neuron projection, and neurotransmitter transport, such as *NeuroD2*, *Dner*, and *Ebf1*.

Knockdown of Chd5 Results in an Upregulation of Polycomb Target Genes

We also identified a smaller cohort of 119 genes that were aberrantly activated in *Chd5*-depleted cells (Figure 3E; Figure S3D). Strikingly, 50 of these genes were previously reported to possess H3K27me3 on their promoters in neurons derived by the same protocol (Mohn et al., 2008), representing a 4-fold enrichment over that expected (Figure 3F). Furthermore, there was a paucity of H3K4me3 promoter-positive genes within the 119 upregulated genes (Figure 3F), again supporting the idea that these genes are ordinarily not expressed during normal neurogenesis. These results suggested that CHD5 might functionally interact with Polycombs during neurogenesis and were reminiscent of the reported functional interplay between dMI-2 and Polycomb in *Drosophila* (Kehle et al., 1998). Interestingly, the cohort of Polycomb target genes that were upregulated in *Chd5*-depleted cells was strikingly rich in factors characteristic of nonneuronal lineages derived from the extraembryonic, mesodermal, and endodermal germ layers (Figure 3E; Figure S3D). Taken together, these data suggest that proper differentiation along the neuronal lineage is dependent on the capacity of CHD5 to facilitate the activation of neuronal gene expression and to maintain the repression of a small cohort of Polycomb-repressed genes.

CHD5 Binds to H3K27me3 via Its Tandem Chromodomains

To investigate the function of the histone-binding domains of CHD5 (Figure 4A), we performed peptide pull-down assays on nuclear lysates generated from either mouse cortices or human SH-SY5Y neuroblastoma cells, and found that endogenous CHD5 protein was enriched on an H3K27me3 peptide compared with an unmodified H3 peptide (Figure 4B; Figure S4). The HP1γ protein strongly bound to H3K9me3, whereas EZH2 was preferentially enriched on H3K27me3, as expected (Bannister and Kouzarides, 2011). To further explore the apparent binding preference of CHD5 to the H3K27me3 modification, we then performed peptide pull-downs of whole-cell lysates from HEK293 cells transfected with FLAG-tagged recombinant proteins representing the histone-binding regions of CHD5 (Figure 4C). This

confirmed that the histone-binding domain region of CHD5 is both necessary and sufficient to mimic the H3K27me3 binding preference of the full-length CHD5 protein, and that, as expected, a CHD1 fragment enriched on the H3K4me3 peptide. Notably, CHD5 fragments with point mutations in either of the two chromodomains had reduced affinity to the H3K27me3 peptide (Figure 4C).

We next purified recombinant glutathione S-transferase (GST) fusion protein fragments, representing the putative histone-binding domain regions of CHD5 and CHD1, and performed peptide pull-downs in a cell-free context (Figure 4D). The GST-tagged wild-type CHD5 fragment bound to the H3 peptide and preferentially bound H3K27me3 (Figure 4D). Interestingly, this fragment did not bind to the H3K4me3 peptide, consistent with the previous demonstrated ability of the PHDs of CHD5 to discriminate against H3K4 when it is in the trimethylated state (Paul et al., 2013). Importantly, the control GST-CHD1 fragment enriched on the H3K4me3 peptide (Figure 4D). We tested an equivalent CHD5 fragment with two point mutations (one in each chromodomain), denoted GST-CHD5 (L518A/Y619E), and found that it displayed a loss of preferential enrichment on the H3K27me3 peptide compared with the unmodified H3 peptide. Finally, in order to directly test the ability of the CHD5 chromodomains to bind H3K27me3, we generated another recombinant protein, denoted GST-CHD5-chromodomains (representing only the two chromodomains of CHD5), and performed surface plasmon resonance (SPR) to accurately measure its in vitro binding to H3K27me3 and unmodified H3 peptides (Figure 4E). This analysis revealed that the binding of GST-CHD5-chromodomains to H3K27me3 was highly reproducible, with an apparent K_D of ~1 nM, as determined from independent measurements at four different concentrations of the protein. Taken together, these data demonstrate that CHD5 depends on its chromodomains for its ability to read the H3K27me3 modification.

Genome-wide ChIP-Seq of CHD5 Reveals that It Is Associated with a Large Cohort of Genes

To explore a possible role of CHD5 in regulating gene expression, we performed a genome-wide analysis of CHD5 localization. We utilized human SH-SY5Y neuroblastoma cells, which retain both alleles of *CHD5* and respond to retinoic acid (RA) treatment with upregulation of *CHD5* expression and concomitant acquisition of differentiated neuronal properties (Figure S5A). To unequivocally confirm the specificity of our CHD5 antibody, we took advantage of a biotin-tagging strategy for performing ChIP experiments, known as bioCHIP (Kim et al., 2009). SH-SY5Y cells expressing biotin ligase (BirA) were transfected with either a plasmid expressing Avidin-tagged CHD5 (FBio-CHD5) or a control empty vector (FBio-Ctrl). ChIP-seq with our endogenous CHD5 antibody was performed in parental RA-treated SH-SY5Y cells, whereas bioChIP-seq was performed in both the FBio-Ctrl- and FBio-CHD5-expressing, RA-treated SH-SY5Y cell lines, respectively. This analysis, represented in heatmap format, demonstrated that the binding profile of the endogenous CHD5 ChIP-seq experiment was highly comparable to that of the bio-CHD5 ChIP-seq experiment (Figure 5A). Interestingly, the pattern of CHD5 binding varied from gene to gene, but was generally broadly localized across gene loci (Figure 5B). Surprisingly, despite our demonstration of the ability of the chromodomains of CHD5 to bind to the H3K27me3 mark (Figure 4), the majority of CHD5 target genes lacked H3K27me3 (Figure 5A). In total, CHD5 bound around the promoter regions of 12,220 genes without H3K37me3, while another 708 CHD5-bound genes were focally enriched with H3K27me3 on their promoters. Intriguingly, a GO analysis of this cohort of 708 CHD5/H3K27me3 double-positive genes revealed that they were primarily enriched for transcriptional regulators and genes involved in developmental signaling pathways of nonneuronal lineages, most prominently of the mesodermal germ layer (Figure S5B). In contrast, the CHD5-only genes were most significantly enriched for genes of the nerve-growth-receptor signaling pathway. To validate the ChIP-seq experiments, we performed independent ChIP-qPCR experiments and confirmed CHD5 binding on five CHD5-only and ten CHD5/H3K27me3 double-positive genes, but not on two H3K27me3-only genes (Figure 5C).

CHD5 Associates with Neuronal Genes and Is Required for Their Activation during Neurogenesis

To determine whether the presence of CHD5 on genes encoding neuronal regulators is required for their activation during neurogenesis, we stably transduced SH-SY5Y neuroblastoma cells with either *shCtrl* or *shCHD5* constructs and treated them for 8 days with 10 μM RA (Figure 6A). In contrast to the *shCtrl*-transduced cells, SH-SY5Y cells transduced with the *shCHD5* construct did not upregulate *CHD5* or *TUBB3* expression after RA treatment (Figures 6B and 6C). They instead maintained a high rate of proliferation and failed to acquire a neuronal morphology (Figure 6A). This suggested that CHD5 is required for neuronal differentiation of human neuroblastoma cells and is consistent with our earlier observations of a similar requirement both in the developing murine neocortex and in mouse ESCs (Figures 2 and 3).

We next tested the mRNA expression levels of three additional CHD5-only target genes that are known to be expressed within the differentiating sympathoadrenal lineage: *PHOX2A, RARA*, and *TBX2* (Boskovic and Niles, 2004; Harrelson and Papaioannou, 2006; Joshi et al., 2006). These genes were all upregulated in the *shCtrl* cells after RA treatment, but not in the *CHD5*-depleted cells (Figure 6C). We also performed CHD5 and H3K27me3 ChIP-qPCRs on these genes and found that the association of CHD5 on their promoters correlated with their upregulation during neurogenesis (Figure 6D). Taken together with our previous experiments, these results suggest that CHD5 is required to facilitate the activation of the several crucial neuronal genes and is directly associated with their gene loci during neuronal differentiation.

The Association of CHD5 with a Cohort of Polycomb Target Gene Loci Is Necessary to Maintain Their Repressed State during Neurogenesis

To explore the potential role of CHD5 in the repression of Polycomb target genes, we monitored the mRNA expression of four CHD5/H3K27me3 double-positive genes (*HES7*, *DLX2*, *WNT7A*, and *EPAS1*) before and after RA treatment in *shCtrl* and *shCHD5* cells (Figure 6E). Strikingly, all four genes were aberrantly activated in the absence of CHD5. This correlated with depletion of CHD5 on their gene promoters and a

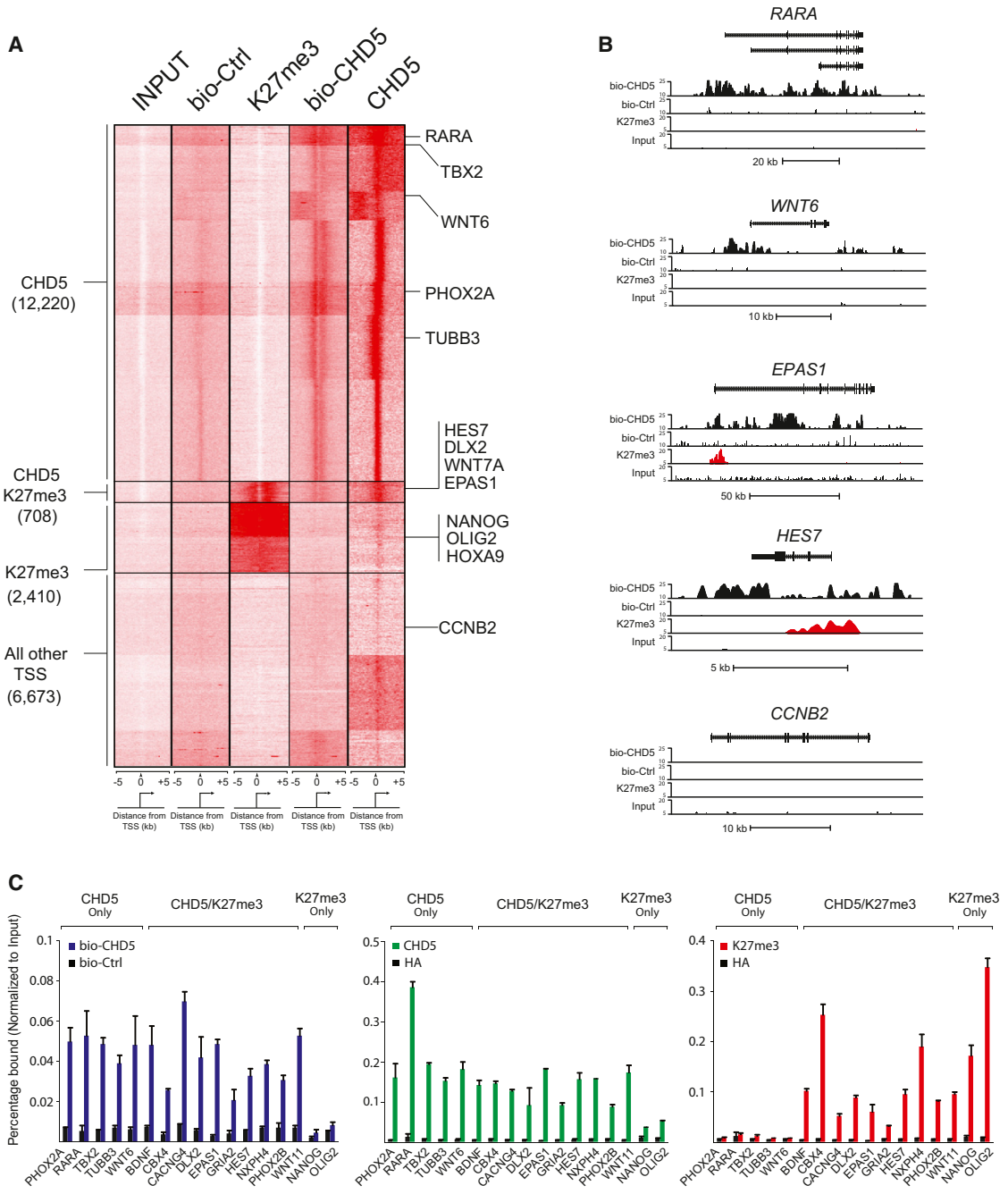

Figure 5. Genome-wide ChIP-Seq Analysis of CHD5 and H3K27me3 in Differentiated SH-SY5Y Cells

(A) Heatmap representation of the read frequency (±5 kb around all transcription start sites) obtained from ChIP-seq and bioChIP-seq experiments of input DNA (FBio-CHD5 expressing SH-SY5Y cells), bio-Ctrl, K27me3 (FBio-CHD5 expressing SH-SY5Y cells), bio-Chd5, and endogenous CHD5 (SH-SY5Y cells). All cells lines were treated with 10 μM RA for 8 days prior to ChIP experiments.

(B) Representative examples of bio-CHD5 and H3K27me3 ChIP-seq tracks for the four indicated CHD5 target genes. The *CCNB2* gene is shown as a negative control.

(C) ChIP and bioChIP qPCR validation analysis with the indicated antibodies on a panel of CHD5 target genes in differentiated FBio-CHD5-expressing SH-SY5Y cells. The precipitated DNA was analyzed by qPCR with primers corresponding to the promoter regions of the indicated genes and presented as the percentage of protein bound, normalized to input. Error bars indicate the SD of triplicate qPCR data.

See also Figure S5.

concomitant loss in the levels of H3K27me3 (Figure 6F). These results are consistent with three previous studies that established that CHD4, or other members of the NuRD complex, are required for the sustained association of Polycombs on a cohort of cobound target genes in different cell types (Morey et al., 2008; Reynolds et al., 2012; Sparmann et al., 2013) We now

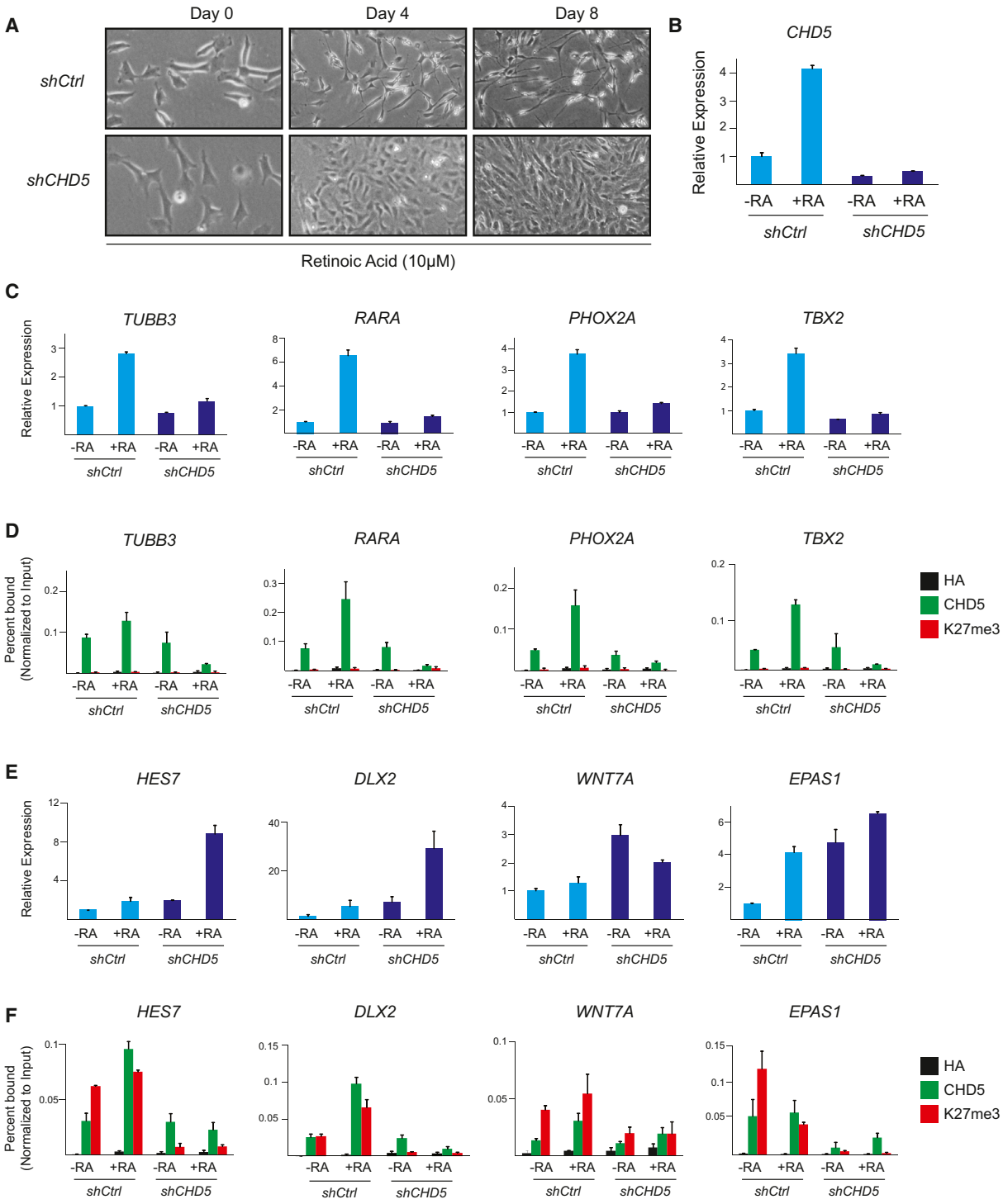

Figure 6. CHD5 Is Required for Differentiation of SH-SH5Y Cells, Activation of Neuronal Genes, and Repression of Polycomb Target Genes

(A) Phase-contrast microscopy of SH-SY5Y cells infected with either *shCtrl*- or *shCHD5*-expressing lentivirus and induced to differentiate for 8 days in the presence of 10 μM RA.

(B) qRT-PCR analysis of *CHD5* mRNA levels in *shCtrl*- and *shCHD5*-infected SH-SY5Y cells before and after 8 days of differentiation in RA.

(C) qRT-PCR analysis of the indicated CHD5 target genes in the presence or absence of CHD5, before and after RA-induced differentiation.

(D) ChIP analysis with the indicated antibodies on the same genes as in (C).

(E) qRT-PCR analysis of the indicated double-positive CHD5/H3K27me3 genes before and after RA-induced differentiation in the presence or absence of CHD5.

(F) ChIP analysis with the indicated antibodies on the same genes as in (E).

Error bars indicate the SD of triplicate qPCR data.

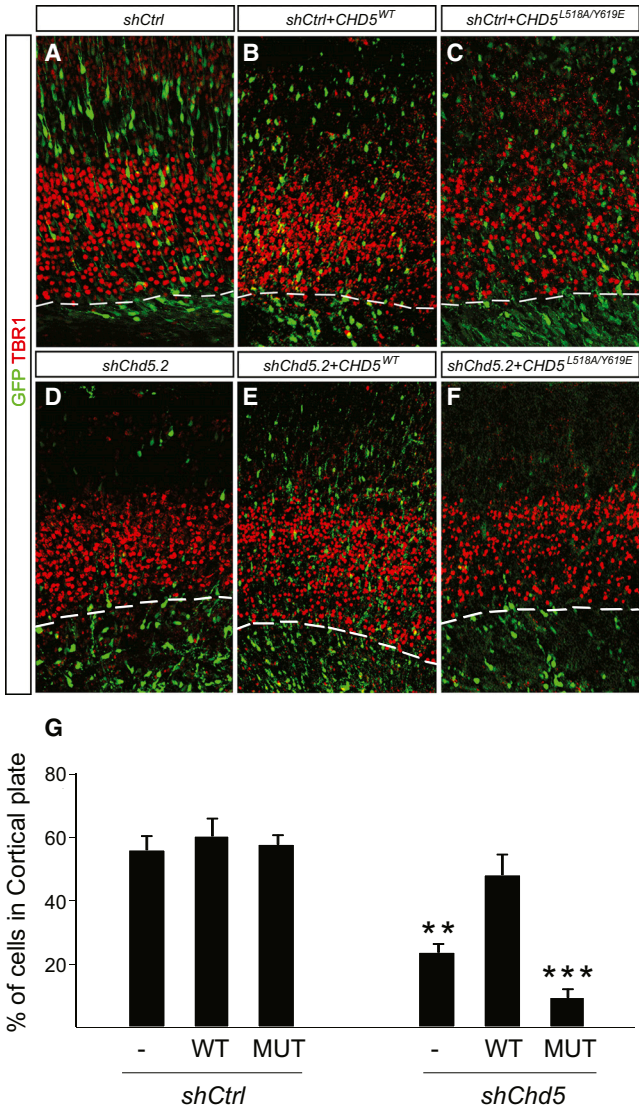

Figure 7. The Chromodomains of CHD5 Are Required for Its Role during Embryonic Cortical Differentiation

(A–C) In utero electroporated *shCtrl-Gfp*-expressing cells (green) migrate into the cortical plate through the TBR1$^+$ (red) layers V–VI (A). This pattern of differentiation is not disrupted by combined expression with *shCtrl-Gfp* and the wild-type full-length human CHD5, *CHD5-FL* (B), or with the mutated CHD5 construct, *CHD5*$^{L518/Y619E}$ (C).

(D) Cells electroporated with *shChd5.2-Gfp* (green) do not migrate into the TBR1$^+$ (red) cortical plate.

(E) The expression of *CHD5-FL* with *shChd5.2-Gfp* restores a normal pattern of differentiation.

(F) The expression of *CHD5*$^{L518/Y619E}$ fails to rescue the *shChd5.2-Gfp* phenotype.

(G) Quantification of the percentage of GFP$^+$ cells that are located in the cortical plate, as determined by the TBR1$^+$ region and above (dashed line in A–F).

Data are represented as mean ± SEM. **p < 0.01, ***p < 0.001, ANOVA with a Newman-Keuls multiple-comparisons posttest, n = 5–12.

demonstrate that CHD5, like CHD4, is required to facilitate the deposition of H3K27me3 on a cohort of Polycomb target genes during differentiation.

The Chromodomains of Chd5 Are Required for Neuronal Differentiation

To determine whether the H3K27me3-binding chromodomains are important for the functional role of CHD5 during neuronal differentiation, we performed an in vivo rescue experiment with double electroporations at E14.5, with either *shCtrl-Gfp* or *shChd5.2-Gfp*, in combination with a vector expressing either wild-type human full-length CHD5 (CHD5-FL) or a full-length CHD5 mutant with two amino acid substitutions within the chromodomains, which are required for binding H3K27me3 (CHD5-L518A/Y619E). We observed that neither CHD5-FL nor CHD5-L518A/Y619E had any detectable effect on the *shCtrl-Gfp*-expressing cells (Figures 7A–7C and 7G). The fact that overexpression of CHD5-FL did not promote premature cell-cycle exit or induce neuronal differentiation suggests that CHD5 lacks inductive capacity and plays a more permissive, albeit essential, role during neurogenesis (Figure 7B). The combined electroporation of *CHD5-FL* with *shChd5.2-Gfp* efficiently rescued the CHD5 knockdown phenotype (Figures 7D, 7E, and 7G). In contrast, CHD5-L518A/Y619E failed to restore a normal pattern of neuronal differentiation when it was coelectroporated with *shChd5.2-Gfp*, even though it was expressed at levels comparable to those observed for the CHD5 FL construct (Figures 7F and 7G; data not shown). These results suggest that the chromodomains of CHD5, and possibly their interaction with H3K27me3, are required for terminal neuronal differentiation.

DISCUSSION

Here we report that the chromatin remodeler CHD5 is required for terminal differentiation of neuronal progenitors. Genome-wide ChIP-seq analysis revealed that CHD5 binds a large cohort of genes and is required to facilitate the activation of neuronal genes during neuronal differentiation. We also show that the localization of CHD5 on a cohort of Polycomb target genes is necessary to maintain their repressed state. The chromodomains of CHD5 bind to H3K27me3 and are essential for neurogenesis. Taken together, our data support a model in which CHD5 has a permissive but essential role during neurogenesis, in which it both facilitates the activation of neuronal genes and synergizes with Polycomb group proteins to facilitate the repression of genes encoding regulators of alternative lineages.

We observed that the overexpression of CHD5 failed to promote neurogenesis (Figure 7B), suggesting that it lacks the inductive capacity of proneural bHLHs such as Ascl1 and Neurogenin 2 (Bertrand et al., 2002). Interestingly, the Trithorax group protein MLL1, which also lacks instructive ability, was shown to facilitate activation of the proper gene expression program during neurogenesis (Lim et al., 2009). It is not known how CHD5 and MLL1 are recruited to their target genes. However, it may involve the association with lineage-specific transcription factors and/or long noncoding RNAs. The precise mechanism(s) by which CHD5 (and CHD3 and CHD4, for that matter) facilitates the activation of gene expression remain unclear. One hypothesis is that the associated histone deacetylase (HDAC) activity of NuRD-like complexes is required to suppress spurious transcription initiation on actively transcribed genes (Reynolds et al., 2013). Another idea is that NuRD and CHD5-NuRD-like complexes may be associated with genes in order to "prime"

them for rapid gene activation. A third possibility is that these proteins are involved in the ''dampening'' of expression on these active genes, and their failure to become activated is the secondary consequence of the inappropriate activation of other CHD5 target genes (Reynolds et al., 2012). It is clear that the role of CHD3–5 and dMI-2 on active gene loci requires further investigation.

We also demonstrate that CHD5 is required for the silencing of a cohort of Polycomb target genes. This functional interplay between CHD5 and Polycombs may be part of an evolutionary conserved process. For example, the *Drosophila* dMI-2 and mammalian CHD4 proteins both functionally interact with Polycombs to maintain the repressed state of certain genes (Kehle et al., 1998; Reynolds et al., 2012; Sparmann et al., 2013). Some mechanistic clues as to the nature of this interplay have come from recent work by Reynolds et al. (2012), who showed that the loss of NuRD-mediated histone deacetylation activity in *Mbd3* null cells correlated with a loss of JARID2 and SUZ12 association on CHD4 target genes. The authors speculated that the deacetylation activity of NuRD is required for the deposition of PRC2-mediated H3K27me3. Since CHD5 has also been shown to be part of a large multiprotein complex containing MBD3 and HDAC2 (Potts et al., 2011), it is possible that CHD5 also recruits deacetylase activity to Polycomb target genes. In support of such a role for a CHD5 complex in the mediation of H3K27me3, we show that the depletion of CHD5 leads to a loss of H3K27me3 on the gene loci of CHD5/H3K27me3 double-positive genes (Figure 6).

The binding of CHD5 to H3K27me3 suggests that it contributes to the silencing of nonneuronal genes (Figure 4). We show that a CHD5 protein with two point mutations in its two chromodomains was incapable of rescuing neurogenesis in the developing neocortex (Figure 7). CHD5 contains two PHDs and two chromodomains, which we propose act synergistically to determine its histone-binding specificity. CHD5 preferentially binds H3K27me3 and mutation of either of its two chromodomains perturbs this preference. It is likely that the residual binding capacity of CHD5 to histone H3 is mediated by its PHDs, as reported previously (Paul et al., 2013). Consistent with this, both chromodomain mutants retain their ability to discriminate against the H3K4me3 mark and bind the H3 tail. Two key features of this work on the histone binding are worth highlighting. First, we assayed the combined histone reading module of CHD5 simultaneously. Second, and crucially, we performed the binding studies with custom synthesized peptides that contained both the H3K4 and H3K27 epitopes (H3; amino acids 1–40), thereby allowing both the PHD and chromodomains to interact with the peptide. This allowed us to show that the N-terminal region of CHD5 constitutes a multivalent histone recognition cassette, with independent histone reading functions attributed to both the tandem PHD and tandem chromodomains. Given the structural similarities between CHD5 and CHD3/CHD4, this implies that the chromodomains of the CHD3 and CHD4 proteins might have similar importance for their respective functions.

Our results also have implications for our understanding of neuroblastoma. We speculate that the loss of CHD5 contributes to tumor formation, at least in part, by rendering neuroblasts incapable of undergoing terminal differentiation. Supporting this, the ability of human neuroblastoma cells to undergo neuronal differentiation upon prolonged exposure to RA is associated with retained 1p36 status (Figure S5A). Indeed, the knockdown of CHD5 in SH-SH5Y neuroblastoma cells led to a complete block in their ability to undergo RA-induced differentiation and a failure to upregulate neuronal gene expression (Figures 6A and 6C). RA treatment has been shown to improve survival in certain treatment regimens of neuroblastoma (Matthay et al., 1999). Interestingly, CHD5 expression is usually maintained in spontaneously regressing infant neuroblastomas (Garcia et al., 2010). Since regression is also associated with differentiation, we speculate that the retained ability to express *CHD5* in these neuroblastomas renders them responsive to RA-induced differentiation (Figures 6A; Figure S5A). It is possible that the 1p36 deletions render cells incapable of differentiating, but these cells would also need an additional oncogenic mutation to drive cellular proliferation, such as *MYCN* amplification (Caron et al., 1993). Indeed, 1p36 deletions are frequently accompanied by *MYCN* amplifications (Brodeur, 2003). Furthermore, we observe that upon *Chd5* knockdown, progenitor cells retain several undifferentiated characteristics but exhibit only a modestly increased level of proliferation (Figures 2G and 2I). From a clinical perspective, this implies that the status of CHD5 expression is a factor that one should take into account when deciding whether or not to treat a neuroblastoma patient with RA. In addition, strategies to reactivate CHD5 expression, such as DNA demethylating agents, might prove useful for increasing the effectiveness of RA in patients with epigenetic silencing of one or two *CHD5* alleles.

On a broader level, the deregulation of the H3K27me3 mark is emerging as a common feature of cancer that appears to be context dependent. For instance, EZH2 was recently reported to have gain-of-function mutations in human B cell lymphomas that correlate with elevated levels of H3K27me3 (Morin et al., 2010; Yap et al., 2011). The H3K27me3 demethylase UTX is frequently inactivated by a variety of deletions, truncations, and frame-shift mutations in many different types of cancer (van Haaften et al., 2009). EZH2 has also been reported to be deleted and have inactivating mutations in certain myeloid leukemias (Ernst et al., 2010; Nikoloski et al., 2010), and the histone H3 residue H3K27 is itself mutated in juvenile glioblastomas (Schwartzentruber et al., 2012). Intriguingly, our results suggest that deletion of *CHD5* in neuroblastoma is another example of H3K27me3 deregulation.

Further studies will be required to determine the functional importance of the binding of CHD5 chromodomains to H3K27me3 and whether this is essential for terminal differentiation of neuronal progenitors. In summary, these results provide a deeper understanding of the function of CHD5. Furthermore, they suggest that the loss of *CHD5* contributes to neuroblastoma via a defect in neuronal differentiation.

EXPERIMENTAL PROCEDURES

Peptide Pull-Down Assay

For peptide pull-down experiments, 1 μg of either unmodified or modified biotinylated H3 peptides containing the amino acid sequence ARTKQTARK STGGKAPRKQLATKAARKSAPATGGVKKPHR-YCK were first coupled to streptavidin agarose beads (Invitrogen) in high salt (HS) buffer for 2 hr at 4°C (50 mM Tris-HCl, pH 7.5, 300 mM NaCl, 0.1% (v/v) NP-40, 1 mM

phenylmethanesulfonylfluoride [PMSF]). The beads were washed three times in HS buffer, and cell or nuclear lysates were incubated with the beads for an additional 2 hr. The beads were then washed four times with HS buffer, and bound proteins were separated on SDS-PAGE gels in Laemmli buffer.

Preparation of Nuclear Protein Lysates

Cells were harvested, washed three times in PBS, and resuspended in ice-cold nuclear extraction buffer (10 mM Tris-HCL (pH 8.0), 100 mM NaCl, 2 mM $MgCl_2$, 0.3 M sucrose, 0.25% (v/v) NP40, 1 μg/ml aprotinin, 10 μg/ml leupeptin, and 1 mM PMSF). The mixture was transferred to an ice-cold dounce for five stokes with a tight-fitting pestle and then transferred to a 15 ml tube and centrifuged at 4,000 rpm at 4°C for 10 min. The supernatant was discarded and the nuclear pellet was solubilized in HS buffer (50 mM Tris-HCl, pH 7.5, 300 mM NaCl, 0.1% (v/v) NP-40, 1 mM PMSF), precleared by centrifugation at 14,000 rpm at 4°C for 10 min, quantified, and used in either western blot or peptide pull-down assays.

Western Blot Analysis

Cell pellets were lysed with HS buffer (300 mM NaCl, 50 mM Tris pH 7.2, 0.5% Igepal CA630, 1 mM EDTA, pH 7.2), 10 μM leupeptin, 0.3 μM aprotinin, and 1 mM PMSF. Lysates were sonicated 2 × 10 s at 10% amplitude and cleared by centrifugation at 20,000 × *g* for 30 min at 4°C. Laemmli sample buffer (125 mM Tris-Cl [pH 6.8], 4% [w/v] SDS, 20% [v/v] glycerol, 0.02% [w/v] bromophenol blue) and dithiothreitol (DTT) were added to the lysates (final concentration of 100 mM) and an equal amount of protein was loaded onto SDS-PAGE gels (BioRad). Subsequently, the proteins were transferred to a Hybond-C extra membrane (Amersham) and blocked in 5% milk in PBS-T (PBS with 0.1% Tween-20), followed by primary antibody incubation for 1–2 hr at room temperature. Anti-mouse or anti-rabbit horseradish peroxidase (HRP)-coupled secondary antibody (Vector Laboratories) was added in 1:10,000 dilution and incubated for 1 hr. Supersignal West Pico (Thermo Scientific) was used as chemical substrate.

Quantification of mRNA Levels by qPCR

Complementary DNA was generated by RT-PCR using the PE Applied Biosystems TaqMan reverse transcription reagents. Reactions were determined using the SYBR Green I detection chemistry system (Applied Biosystems) and an ABI Prism 7300 sequence detection system. RPO was used as a control gene for normalization. The sequences of the primers used in this study are available upon request.

Agilent Expression Analysis

Total RNA was extracted using the RNeasy Plus Mini Kit (QIAGEN). For each treatment, RNA was prepared from three independent experiments and pooled into one sample. Samples for microarray hybridization were synthesized accordingly to the supplier's instructions (Agilent). The 44K whole mouse gene expression microarray, which interrogates all annotated transcripts in the mouse genome, was used for gene expression profiling. For each time point, two independent arrays were hybridized with pooled complementary RNA. Hybridization, washing, staining, scanning, and data analysis were performed according to the manufacturer's instructions. Expression levels were analyzed using the Genespring software program. Tree-view diagrams were generated using the online resource Matrix2png (Pavlidis and Noble, 2003). GO analysis was performed with FuncAssociate 2.0 (Berriz et al., 2009).

Surface Plasmon Resonance

K27me3 and H3 peptides from 500 nM stock solutions were injected in 1 min pulses at 10 μl/min in HBS running buffer (10 mM HEPES, 150 mM NaCl, 0.005% Tween) onto individual streptavidin-coated flow cells of a series S SA sensor chip until 1,000 RU peptide was immobilized on each flow cell, with a blank flow cell used for reference subtraction on a BiaCore T200 instrument. GST-CHD5-chromodomains was diluted in running buffer to working concentrations of 2, 4, 8, and 16 nM. They were injected for 180 s to measure the association constants, and the dissociation was followed for 300 s to measure the off rate. The K_D was determined using a 1:1 Langmuir fit of these sensorgrams.

In Utero Knockdown of Chd5

Pregnant (E14) CD1 mice were anesthetized with isoflurane, the uterine horns were exposed, and 1–1.5 μl of plasmid DNA (2–6 μg/μl) in PBS with fast green (2 mg/ml; Sigma) was microinjected with glass microcapillaries into the lateral ventricles of the embryos. Five electric pulses of 50 V for 50 ms were discharged at intervals of 950 ms across the head using an electroporator (Nepagen CUY21D) and platinum electrodes (Nepagene Cuy650P5). Embryos were retrieved at E18.5, and the brains were dissected and fixed in 4% paraformaldehyde (PFA) overnight at 4°C. After overnight cryoprotection in 30% sucrose, the brains were cryosectioned onto Superfrost Plus slides (Thermo Scientific).

Immunostaining

Cells and tissues were fixed in 4% PFA, blocked, and permeabilized in 5% BSA in PBS-T (PBS with 0.2% Tween-20), followed by primary antibody incubation in a cold room overnight using the following antibodies: rabbit anti-CHD5 directed at the C or N terminus at 1:500 (see below); mouse anti-NEUN at 1:1,000 (Millipore); mouse anti-TUJ1 at 1:1,000 (Covance); goat anti-DCX at 1:500 (Santa Cruz Biotechnologies [SCBT]); mouse anti-pH3 at 1:1,000 (Upstate Biotechnologies), guinea pig anti-SOX3 at 1:1,000 (a kind gift from J. Muhr); rabbit anti-MAP2 1:1,000 (Millipore); rabbit anti-CHD3/4 1:200 (SCBT); mouse anti-PCNA at 1:400 (Oncogene); rabbit anti-CUX1 at 1:500 (SCBT); and mouse anti-S100β, mouse anti-APC at 1:500, mouse anti-GFAP at 1:100, rat anti-BrdU at 1:250, mouse anti-TBR1 at 1:500, mouse anti-SATB2 at 1:100, and rabbit anti-Ki67 at 1:500 (all from Abcam). Alexa Fluor-488, Alexa Fluor 555, and Alexa Fluor 647 coupled secondary antibody (Life Technologies) was added in 1:1,000 dilution and incubated for 1 hr. Images were taken with a LSM5 Exciter confocal microscope (Zeiss) and analyzed with Photoshop CS5 (Adobe).

ChIP, BioChIP, and High-Throughput Sequencing

ChIP assays were carried out as described previously with minor modifications (Bracken et al., 2006). Briefly, cells were crosslinked with ethylene glycol bis(succinimidylsuccinate) for 45 min at room temperature, washed with PBS, and further incubated with 1% formaldehyde for 10 min at room temperature. Crosslinked chromatin was fragmented by sonication to an average size of 200–350 bp and immunoprecipitated overnight with 1–10 μg of the indicated antibodies. For bioChIP, SH-SY5Y cells expressing either FBio-Ctrl or FBio-CHD5 constructs (~8×10^7 cells) were differentiated in 10 μM of RA for 8 days. Sonicated chromatin was precleared with Protein A beads and then incubated with 50 μl of streptavidin beads (Dynabeads Streptavidin M280) at 4°C overnight. Wash and elution steps were carried out following the protocol described in Kim et al., (2009). ChIP DNA was then quantified and used for library preparation using a standard ChIP-seq sample preparation kit (Illumina). ChIP-seq library DNA was sequenced on an Illumina HiSeq 2000 platform (BGI genomics). Base calling and mapping of the 50 bp sequence reads to the human genome (hg19, February 2009 release) was performed using the burrows-wheeler alignment tool, allowing for up to two mismatches in each read. Peak detection was performed using MACS (Zhang et al., 2008) and the FBio-Ctrl data set served as a control for normalization. Heatmaps were generated using the seqMINER algorithm (Ye et al., 2011).

For further details regarding the materials and methods used in this work, see the Supplemental Experimental Procedures.

ACCESSION NUMBERS

Data sets are available for download from NCBI's Gene Expression Omnibus (GEO, http://www.ncbi.nlm.nih.gov/geo) through series accession number GSE48314.

SUPPLEMENTAL INFORMATION

Supplemental Information includes Supplemental Experimental Procedures and five figures and can be found with this article online at http://dx.doi.org/10.1016/j.devcel.2013.07.008.

ACKNOWLEDGMENTS

We are indebted to J. Frisén, J. Ericson, J. Muhr, G. Cagney, and members of the Bracken and Holmberg laboratories for valuable comments on the manuscript. We thank Stuart Orkin and Diego Pasini for generous donations of the pEF1-BirAV5-neo and pFBio-Empty plasmids, respectively. We also thank Karsten Hokamp, TCD, for bioinformatic support. Work in the Bracken laboratory is supported by Science Foundation Ireland under a Principal Investigator Career Advancement Award (SFI PICA SFI/10/IN.1/B3002) and the Health Research Board under Health Research Awards 2010 (HRA_POR/2010/124). Work in the Holmberg laboratory is supported by grants from the Swedish Cancer Society, the Swedish Research Council, the L. Sagens och C. Eriksons Stift, DBRM, and Swedish Childhood Cancer Foundation. U.N. was supported by a postdoctoral fellowship from the Swedish Cancer Society. Work in the Helin laboratory was supported by the Danish National Research Foundation, the Lundbeck Foundation, and the Novo Nordisk Foundation.

Received: December 28, 2011
Revised: April 2, 2013
Accepted: July 15, 2013
Published: August 12, 2013

REFERENCES

Bagchi, A., Papazoglu, C., Wu, Y., Capurso, D., Brodt, M., Francis, D., Bredel, M., Vogel, H., and Mills, A.A. (2007). CHD5 is a tumor suppressor at human 1p36. Cell *128*, 459–475.

Bajpai, R., Chen, D.A., Rada-Iglesias, A., Zhang, J., Xiong, Y., Helms, J., Chang, C.P., Zhao, Y., Swigut, T., and Wysocka, J. (2010). CHD7 cooperates with PBAF to control multipotent neural crest formation. Nature *463*, 958–962.

Bannister, A.J., and Kouzarides, T. (2011). Regulation of chromatin by histone modifications. Cell Res. *21*, 381–395.

Berriz, G.F., Beaver, J.E., Cenik, C., Tasan, M., and Roth, F.P. (2009). Next generation software for functional trend analysis. Bioinformatics *25*, 3043–3044.

Bertrand, N., Castro, D.S., and Guillemot, F. (2002). Proneural genes and the specification of neural cell types. Nat. Rev. Neurosci. *3*, 517–530.

Bibel, M., Richter, J., Lacroix, E., and Barde, Y.A. (2007). Generation of a defined and uniform population of CNS progenitors and neurons from mouse embryonic stem cells. Nat. Protoc. *2*, 1034–1043.

Boskovic, G., and Niles, R.M. (2004). T-box binding protein type two (TBX2) is an immediate early gene target in retinoic-acid-treated B16 murine melanoma cells. Exp. Cell Res. *295*, 281–289.

Bracken, A.P., and Helin, K. (2009). Polycomb group proteins: navigators of lineage pathways led astray in cancer. Nat. Rev. Cancer *9*, 773–784.

Bracken, A.P., Dietrich, N., Pasini, D., Hansen, K.H., and Helin, K. (2006). Genome-wide mapping of Polycomb target genes unravels their roles in cell fate transitions. Genes Dev. *20*, 1123–1136.

Breunig, J.J., Silbereis, J., Vaccarino, F.M., Sestan, N., and Rakic, P. (2007). Notch regulates cell fate and dendrite morphology of newborn neurons in the postnatal dentate gyrus. Proc. Natl. Acad. Sci. USA *104*, 20558–20563.

Brodeur, G.M. (2003). Neuroblastoma: biological insights into a clinical enigma. Nat. Rev. Cancer *3*, 203–216.

Caron, H., van Sluis, P., van Hoeve, M., de Kraker, J., Bras, J., Slater, R., Mannens, M., Voûte, P.A., Westerveld, A., and Versteeg, R. (1993). Allelic loss of chromosome 1p36 in neuroblastoma is of preferential maternal origin and correlates with N-myc amplification. Nat. Genet. *4*, 187–190.

Clapier, C.R., and Cairns, B.R. (2009). The biology of chromatin remodeling complexes. Annu. Rev. Biochem. *78*, 273–304.

Ernst, T., Chase, A.J., Score, J., Hidalgo-Curtis, C.E., Bryant, C., Jones, A.V., Waghorn, K., Zoi, K., Ross, F.M., Reiter, A., et al. (2010). Inactivating mutations of the histone methyltransferase gene EZH2 in myeloid disorders. Nat. Genet. *42*, 722–726.

Flanagan, J.F., Mi, L.Z., Chruszcz, M., Cymborowski, M., Clines, K.L., Kim, Y., Minor, W., Rastinejad, F., and Khorasanizadeh, S. (2005). Double chromodomains cooperate to recognize the methylated histone H3 tail. Nature *438*, 1181–1185.

Fujita, T., Igarashi, J., Okawa, E.R., Gotoh, T., Manne, J., Kolla, V., Kim, J., Zhao, H., Pawel, B.R., London, W.B., et al. (2008). CHD5, a tumor suppressor gene deleted from 1p36.31 in neuroblastomas. J. Natl. Cancer Inst. *100*, 940–949.

Garcia, I., Mayol, G., Rodríguez, E., Suñol, M., Gershon, T.R., Ríos, J., Cheung, N.K., Kieran, M.W., George, R.E., Perez-Atayde, A.R., et al. (2010). Expression of the neuron-specific protein CHD5 is an independent marker of outcome in neuroblastoma. Mol. Cancer *9*, 277.

Gaspar-Maia, A., Alajem, A., Polesso, F., Sridharan, R., Mason, M.J., Heidersbach, A., Ramalho-Santos, J., McManus, M.T., Plath, K., Meshorer, E., and Ramalho-Santos, M. (2009). Chd1 regulates open chromatin and pluripotency of embryonic stem cells. Nature *460*, 863–868.

Harrelson, Z., and Papaioannou, V.E. (2006). Segmental expression of the T-box transcription factor, Tbx2, during early somitogenesis. Dev. Dyn. *235*, 3080–3084.

Ho, L., and Crabtree, G.R. (2010). Chromatin remodelling during development. Nature *463*, 474–484.

Holmberg, J., and Perlmann, T. (2012). Maintaining differentiated cellular identity. Nat. Rev. Genet. *13*, 429–439.

Hu, G., and Wade, P.A. (2012). NuRD and pluripotency: a complex balancing act. Cell Stem Cell *10*, 497–503.

Joshi, S., Guleria, R., Pan, J., DiPette, D., and Singh, U.S. (2006). Retinoic acid receptors and tissue-transglutaminase mediate short-term effect of retinoic acid on migration and invasion of neuroblastoma SH-SY5Y cells. Oncogene *25*, 240–247.

Kehle, J., Beuchle, D., Treuheit, S., Christen, B., Kennison, J.A., Bienz, M., and Müller, J. (1998). dMi-2, a hunchback-interacting protein that functions in polycomb repression. Science *282*, 1897–1900.

Kim, J., Cantor, A.B., Orkin, S.H., and Wang, J. (2009). Use of in vivo biotinylation to study protein-protein and protein-DNA interactions in mouse embryonic stem cells. Nat. Protoc. *4*, 506–517.

Kouzarides, T. (2007). Chromatin modifications and their function. Cell *128*, 693–705.

Lim, D.A., Huang, Y.C., Swigut, T., Mirick, A.L., Garcia-Verdugo, J.M., Wysocka, J., Ernst, P., and Alvarez-Buylla, A. (2009). Chromatin remodelling factor Mll1 is essential for neurogenesis from postnatal neural stem cells. Nature *458*, 529–533.

Margueron, R., and Reinberg, D. (2011). The Polycomb complex PRC2 and its mark in life. Nature *469*, 343–349.

Matthay, K.K., Villablanca, J.G., Seeger, R.C., Stram, D.O., Harris, R.E., Ramsay, N.K., Swift, P., Shimada, H., Black, C.T., Brodeur, G.M., et al.; Children's Cancer Group. (1999). Treatment of high-risk neuroblastoma with intensive chemotherapy, radiotherapy, autologous bone marrow transplantation, and 13-cis-retinoic acid. N. Engl. J. Med. *341*, 1165–1173.

McDonel, P., Costello, I., and Hendrich, B. (2009). Keeping things quiet: roles of NuRD and Sin3 co-repressor complexes during mammalian development. Int. J. Biochem. Cell Biol. *41*, 108–116.

Mohn, F., Weber, M., Rebhan, M., Roloff, T.C., Richter, J., Stadler, M.B., Bibel, M., and Schübeler, D. (2008). Lineage-specific polycomb targets and de novo DNA methylation define restriction and potential of neuronal progenitors. Mol. Cell *30*, 755–766.

Molyneaux, B.J., Arlotta, P., Menezes, J.R., and Macklis, J.D. (2007). Neuronal subtype specification in the cerebral cortex. Nat. Rev. Neurosci. *8*, 427–437.

Morey, L., Brenner, C., Fazi, F., Villa, R., Gutierrez, A., Buschbeck, M., Nervi, C., Minucci, S., Fuks, F., and Di Croce, L. (2008). MBD3, a component of the NuRD complex, facilitates chromatin alteration and deposition of epigenetic marks. Mol. Cell. Biol. *28*, 5912–5923.

Morin, R.D., Johnson, N.A., Severson, T.M., Mungall, A.J., An, J., Goya, R., Paul, J.E., Boyle, M., Woolcock, B.W., Kuchenbauer, F., et al. (2010). Somatic mutations altering EZH2 (Tyr641) in follicular and diffuse large B-cell lymphomas of germinal-center origin. Nat. Genet. *42*, 181–185.

Murawska, M., Kunert, N., van Vugt, J., Längst, G., Kremmer, E., Logie, C., and Brehm, A. (2008). dCHD3, a novel ATP-dependent chromatin remodeler associated with sites of active transcription. Mol. Cell. Biol. *28*, 2745–2757.

Musselman, C.A., Mansfield, R.E., Garske, A.L., Davrazou, F., Kwan, A.H., Oliver, S.S., O'Leary, H., Denu, J.M., Mackay, J.P., and Kutateladze, T.G. (2009). Binding of the CHD4 PHD2 finger to histone H3 is modulated by covalent modifications. Biochem. J. *423*, 179–187.

Nikoloski, G., Langemeijer, S.M., Kuiper, R.P., Knops, R., Massop, M., Tönnissen, E.R., van der Heijden, A., Scheele, T.N., Vandenberghe, P., de Witte, T., et al. (2010). Somatic mutations of the histone methyltransferase gene EZH2 in myelodysplastic syndromes. Nat. Genet. *42*, 665–667.

Okawa, E.R., Gotoh, T., Manne, J., Igarashi, J., Fujita, T., Silverman, K.A., Xhao, H., Mosse, Y.P., White, P.S., and Brodeur, G.M. (2008). Expression and sequence analysis of candidates for the 1p36.31 tumor suppressor gene deleted in neuroblastomas. Oncogene *27*, 803–810.

Paul, S., Kuo, A., Schalch, T., Vogel, H., Joshua-Tor, L., McCombie, W.R., Gozani, O., Hammell, M., and Mills, A.A. (2013). Chd5 requires PHD-mediated histone 3 binding for tumor suppression. Cell Rep. *3*, 92–102.

Pavlidis, P., and Noble, W.S. (2003). Matrix2png: a utility for visualizing matrix data. Bioinformatics *19*, 295–296.

Pietersen, A.M., and van Lohuizen, M. (2008). Stem cell regulation by polycomb repressors: postponing commitment. Curr. Opin. Cell Biol. *20*, 201–207.

Potts, R.C., Zhang, P., Wurster, A.L., Precht, P., Mughal, M.R., Wood, W.H., 3rd, Zhang, Y., Becker, K.G., Mattson, M.P., and Pazin, M.J. (2011). CHD5, a brain-specific paralog of Mi2 chromatin remodeling enzymes, regulates expression of neuronal genes. PLoS ONE *6*, e24515.

Reynolds, N., Salmon-Divon, M., Dvinge, H., Hynes-Allen, A., Balasooriya, G., Leaford, D., Behrens, A., Bertone, P., and Hendrich, B. (2012). NuRD-mediated deacetylation of H3K27 facilitates recruitment of Polycomb Repressive Complex 2 to direct gene repression. EMBO J. *31*, 593–605.

Reynolds, N., O'Shaughnessy, A., and Hendrich, B. (2013). Transcriptional repressors: multifaceted regulators of gene expression. Development *140*, 505–512.

Schnetz, M.P., Bartels, C.F., Shastri, K., Balasubramanian, D., Zentner, G.E., Balaji, R., Zhang, X., Song, L., Wang, Z., Laframboise, T., et al. (2009). Genomic distribution of CHD7 on chromatin tracks H3K4 methylation patterns. Genome Res. *19*, 590–601.

Schübeler, D. (2009). Epigenomics: Methylation matters. Nature *462*, 296–297.

Schuettengruber, B., Martinez, A.M., Iovino, N., and Cavalli, G. (2011). Trithorax group proteins: switching genes on and keeping them active. Nat. Rev. Mol. Cell Biol. *12*, 799–814.

Schwartzentruber, J., Korshunov, A., Liu, X.Y., Jones, D.T., Pfaff, E., Jacob, K., Sturm, D., Fontebasso, A.M., Quang, D.A., Tönjes, M., et al. (2012). Driver mutations in histone H3.3 and chromatin remodelling genes in paediatric glioblastoma. Nature *482*, 226–231.

Simic, R., Lindstrom, D.L., Tran, H.G., Roinick, K.L., Costa, P.J., Johnson, A.D., Hartzog, G.A., and Arndt, K.M. (2003). Chromatin remodeling protein Chd1 interacts with transcription elongation factors and localizes to transcribed genes. EMBO J. *22*, 1846–1856.

Sparmann, A., Xie, Y., Verhoeven, E., Vermeulen, M., Lancini, C., Gargiulo, G., Hulsman, D., Mann, M., Knoblich, J.A., and van Lohuizen, M. (2013). The chromodomain helicase Chd4 is required for Polycomb-mediated inhibition of astroglial differentiation. EMBO J. *32*, 1598–1612.

Taverna, S.D., Li, H., Ruthenburg, A.J., Allis, C.D., and Patel, D.J. (2007). How chromatin-binding modules interpret histone modifications: lessons from professional pocket pickers. Nat. Struct. Mol. Biol. *14*, 1025–1040.

van Haaften, G., Dalgliesh, G.L., Davies, H., Chen, L., Bignell, G., Greenman, C., Edkins, S., Hardy, C., O'Meara, S., Teague, J., et al. (2009). Somatic mutations of the histone H3K27 demethylase gene UTX in human cancer. Nat. Genet. *41*, 521–523.

Yap, K.L., and Zhou, M.M. (2010). Keeping it in the family: diverse histone recognition by conserved structural folds. Crit. Rev. Biochem. Mol. Biol. *45*, 488–505.

Yap, D.B., Chu, J., Berg, T., Schapira, M., Cheng, S.W., Moradian, A., Morin, R.D., Mungall, A.J., Meissner, B., Boyle, M., et al. (2011). Somatic mutations at EZH2 Y641 act dominantly through a mechanism of selectively altered PRC2 catalytic activity, to increase H3K27 trimethylation. Blood *117*, 2451–2459.

Ye, T., Krebs, A.R., Choukrallah, M.A., Keime, C., Plewniak, F., Davidson, I., and Tora, L. (2011). seqMINER: an integrated ChIP-seq data interpretation platform. Nucleic Acids Res. *39*, e35.

Zhang, Y., Liu, T., Meyer, C.A., Eeckhoute, J., Johnson, D.S., Bernstein, B.E., Nusbaum, C., Myers, R.M., Brown, M., Li, W., and Liu, X.S. (2008). Model-based analysis of ChIP-Seq (MACS). Genome Biol. *9*, R137.